Aerosol and Air Quality Research

Effects of Synthesis Conditions on Rare Earth Doped Iron Oxide Catalyst for Selective Catalytic Reduction of NOx with NH3

Ying Wei[1], Bingquan Wang[2], Ruiyi Ren[1], Rui Wang[1*]

[1] School of Environmental Science and Engineering, Shandong University, Qingdao 266237, China
[2] School of Chemistry and Molecular Engineering, Qingdao University of Science and Technology Qingdao 266042, China

ABSTRACT

A series of rare earth-doped Fe-based oxide catalysts were prepared by co-precipitation method as Selective Catalytic Reduction (SCR) catalysts. The effects of the various rare earth species, doping amount of Sm, calcination temperature and the kind of precipitant on the deNOx activity of the catalysts were systematically investigated. The SO2 resistance performance was tested on the optimal catalyst. The catalysts have been characterized by X-ray diffraction (XRD), The X-ray photoelectron spectra (XPS), scanning electron microscopy (SEM) and Brunner Emmet Teller (BET). The results showed that the doping of Sm significantly improves the removal efficiency of Fe-based oxides. $Sm_{0.075}Fe_{0.925}$ catalyst showed the optimal deNOx performance and excellent resistance to SO2. At the optimal doping rate (0.075), the denitrification rate was close to 100% between 200 and 250°C. The calcination temperature has a significant effect on the catalyst. The order of catalytic activity for different calcination temperatures was 350°C ≈ 400°C > 450°C > 500°C. The $Sm_{0.075}Fe_{0.925}$ achieved 100% the de-NOx efficiencies at calcination temperatures of 350–400°C. It was also found that the deNOx performance of the catalyst prepared by using $NH_3 \cdot H_2O$ as the precipitating agent was better than the catalyst prepared by using $(NH_3)_2CO_3$ or NaOH as the precipitating agent. Normally a small amount of SO2 would render the catalyst inactive, but the $Sm_{0.075}Fe_{0.925}$ catalyst was basically regenerated after 0.05% SO2 removal in this resistance test.

Keywords: SCR, Rare earth, Fe oxide, Mesoporous structure, SO2 resistance

1 INTRODUCTION

Nitrogen oxides (NOx) are recognized as one of the main atmospheric pollutants, which are not only the main component of acid rain, but also the culprit in the formation of photochemical smog, acid rain, greenhouse effect and ozone depletion (Eigenmann et al., 2006; Wei, 2014). In terms of economic and technological efficiency, SCR with ammonia is currently the most widely used method for eliminating NOx from stationary sources (France et al., 2017; Chen et al., 2021a). The V_2O_5-WO_3/TiO_2 has been extensively used as a commercial SCR catalyst in the electric plant due to its excellent catalytic activity in the temperature range of 300–400°C (Kroecher and Elsener, 2008; Kompio et al., 2012). However, some shortcomings of this type of catalysts, such as narrow operation temperature window, biological toxicity of active component (V) and poor SO2 resistance, constrain their application (Kobayashi and Miyoshi, 2007; Liu et al., 2009). Therefore, the development of eco-friendly SCR catalyst with high efficiency and high SO2 tolerance is further imperative.

Iron is a low economic cost, and non-toxic transition metal and Fe_2O_3-based catalysts have attracted wide attention in NH3-SCR process because of good medium-high SCR activity, satisfactory
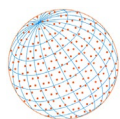
N_2 selectivity, excellent thermal stability and prominent SO_2-tolerant activity at high temperatures (> 300°C), but the operating temperature window of pure FeO_x is narrow (Chen *et al.*, 2018; Han *et al.*, 2019). In recent years, many efforts have been made to develop composite catalyst systems due to the synergetic effects. Therefore, a number of Fe-based catalysts doped with other metal components have been reported. For instance, Yang *et al.* (2011) prepared nanosized Fe-Mn oxide as a super catalyst for the low temperature SCR of NO_x with NH_3. Fan *et al.* (2017) rationally designed the porous nanoneedle-like MnO_x-FeO_x catalyst derived by heat-treating MOFs, which showed excellent NH_3-SCR activity in low temperatures. Fe-Ce mixed oxide catalyst was prepared and the SCR activity at low-temperature over iron oxide was improved significantly by adding a small amount of cerium (Xiong *et al.*, 2013). Besides, the W-modified Fe_2O_3 catalyst can improve the activity and N_2 selectivity in a wider temperature window by tuning surface acidity and redox property (Xin *et al.*, 2018; Wang *et al.*, 2020a; Zhang *et al.*, 2020). The modification of Fe_2O_3 catalyst with Ti species can inhibit the transformation of γ-Fe_2O_3 to α-Fe_2O_3 and weaken the oxidation ability of Fe_2O_3 for the oxidization of NH_3 (Liu *et al.*, 2008; Yang *et al.*, 2013). Besides, many researchers have paid great attention to Fe-exchanged zeolites, i.e., Fe/ZSM-5 (Brandenberger *et al.*, 2011; Ruggeri *et al.*, 2015), Fe/BEA (Shwan *et al.*, 2015, 2012), Fe/SBA-15 (Li *et al.*, 2018).

Rare earth is an important mineral, especially for China. The 5d orbits of electronic structure for most rare earth elements under normal conditions are empty, which can be used as an electron transfer station for catalytic reaction (Da Silva *et al.*, 2016; Xue *et al.*, 2017). Thus, rare earth elements and their oxides have high catalytic activity. Rare earth catalytic materials have been crucial in a number of industries over the years, including petrochemical catalysis, vehicle exhaust catalysis, fuel cell catalysis, catalytic combustion, hydrogen production catalysis, and others (Guo and Lu, 2007; Zhan *et al.*, 2014b). Ce is one of the most common rare earth metals and has been wildly reported as promoter in SCR reaction due to the high oxygen storage/release capacity and superior redox (Shan *et al.*, 2012; Tan *et al.*, 2021). As an important rare earth metal, Sm has also been explored in SCR reaction. Meng *et al.* (2015, 2016) reported that incorporating Sm into the MnO_x catalyst can significantly improve catalytic activity for NH_3-SCR while also improving sulfur and H_2O resistance. Sun *et al.* (2021) found that the incorporation of Sm enhanced adsorption and activation of NH_3 and facilitated the decomposition of NH_4HSO_4.

As well known, the morphology, crystal structure, and nanostructure of oxide catalysts are important to improve the SCR activity, which peculiarly depends on the regulation of their synthesis conditions. In addition, there are a few reports on Sm doped FeO_x catalyst. In this work, rare earth-doped Fe-based oxide catalysts were prepared by the coprecipitation method. The influence of catalyst preparation factors (various rare earth species, doping amount of Sm, calcination temperature and the kind of precipitant) on NH_3-SCR activity were evaluated. In addition, the ability of catalysts for sulfur resistance was also investigated. Various characterizations were used to investigate the effect of Sm addition on the structure and physicochemical properties of FeO_x. These results have important reference value for the optimization of catalyst preparation in further applications.

2 EXPERIMENTAL

2.1 Preparation of Catalysts

The rare earth-doped iron oxide catalysts were prepared by the co-precipitation method. Take SmFe oxide synthesis as an example. Typically, $Fe(NO_3)_3 \cdot 9H_2O$ and $Sm(NO_3)_3 \cdot 6H_2O$ with different stoichiometric ratios were dissolved into deionized water to obtain a uniform solution with a mixed metal cation concentration of 0.2 mole L^{-1}, and then the pH of the solution was adjusted to 8.5–9.5 using alkaline solution (2 mol L^{-1}) containing precipitant ($NH_3 \cdot H_2O$, $(NH_4)_2CO_3$ or NaOH) under vigorous stirring. To remove anion impurities from the formed slurry, it was filtered and washed several times. The crystalline product was dried at 105°C for 12 h and calcined at different temperatures (350, 400, 450 and 500°C) for 5 h in a muffle furnace. The obtained product was denoted as Sm_xFe_{1-x} (x = 0, 0.025, 0.05, 0.075, 0.1). Samples doped with different rare earths were denoted as $Sm_{0.05}Fe_{0.95}$, $Nd_{0.05}Fe_{0.95}$, $Gd_{0.05}Fe_{0.95}$ and $Pr_{0.05}Fe_{0.95}$. The pure FeO_x catalyst was prepared with the same method by comparison.
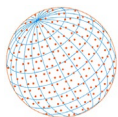
2.2 Catalyst Characterization

XRD patterns were acquired using a BRUKER-AXS D8 Adance X-ray Diffractometer operating at 40 kV and 60 mA with Cu-K radiation (λ = 0.15418 nm). The diffractograms were captured in the 10°–80° scanning angle (2) range with a 0.02° step size.

A Micromeritics Tristar 3020 surface area analyzer was used to measure the surface areas and pore characterization of the catalysts at liquid N_2 temperature (–196°C). The specific surface area, pore size and pore volume were calculated by the multi-point BET method and the BJH model, respectively.

SEM(JSM-6700F) analysis was done on the catalysts' morphological characteristics.

Using Al-Ka radiation, the catalysts were subjected to XPS examination on a scanning X-ray microprobe (PHI5300X). As a standard, the binding energies were calibrated using the C 1s peak (BE = 284.8 eV).

2.3 Activity Measurements

An 8 mm internal diameter fixed-bed quartz tube reactor was used to test the evaluation of catalytic activity. The sample (0.5 g, 40–60 mesh) was fixed with quartz wool in a reactor before being placed in an electric tubular furnace that was temperature-controlled. A simulated reactant gas mixture containing 1000 ppm NO, 1100 ppm NH_3, 6% O_2, 500 ppm SO_2 (when used), and balance N_2 with a gas hourly space velocity (GHSV) of 15,000 h^{-1}. When the reaction reached a stable state at various temperatures, the associated activity statistics were recorded. The TH-990S NO and NO_2 analyzers were used to continuously monitor the amounts of NO and NO_2. The catalytic performance of NH_3-SCR reaction was presented in terms of NO_x conversion calculated as follows:

$$NO_x \text{ conversion } (\%) = \left(1 - \frac{[NO_x]_{out}}{[NO_x]_{in}} \right) \times 100\% \tag{1}$$

where the subscripts "in" and "out" represent the steady-state inlet and output concentrations, respectively.

3 RESULTS AND DISCUSSION

3.1 XRD Analysis

Fig. 1 shows the XRD patterns of Fe-based catalysts with different additions of samarium oxide. All the diffraction peaks observed on FeO_x can be assigned to α-Fe_2O_3 (Jayashree *et al.*, 2019). After the doping of Sm on FeO_x, the intensity of the Fe_2O_3 diffraction peaks in the catalyst gradually decreased with the increase of Sm and the diffraction peak of α-Fe_2O_3 disappeared when the mole ratio of Sm was up to 0.075. It is difficult to observe the diffraction peaks of samarium oxide on all the mixed samples. This phenomenon suggests that samarium oxide and iron oxide interacted vigorously. The addition of Sm affected the nucleation process of iron oxide grains and inhibited the growth of iron oxide particles, reducing the crystallinity of α-Fe_2O_3. This means that the iron and samarium components form a solid solution with amorphous state.
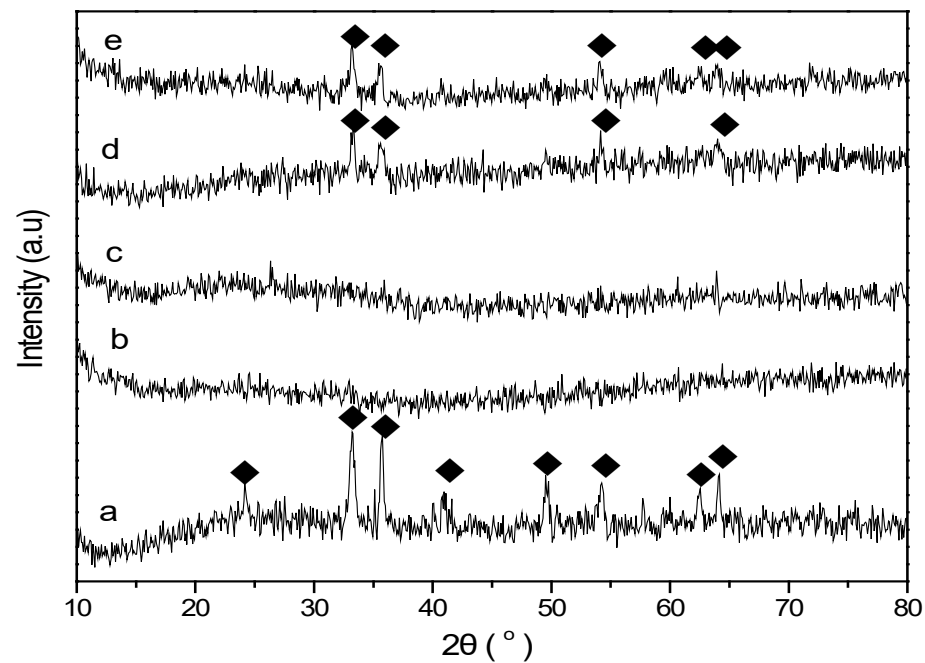
Fig. 2 shows the XRD patterns of $Sm_{0.075}Fe_{0.925}$ catalysts calcined at different temperatures. For the catalysts calcined at 350°C and 400°C, no diffraction peaks of iron oxide and samarium oxide were found. It can be seen that the diffraction peaks of Fe_2O_3 can be observed when the calcination temperature rises to 450°C. The diffraction peak of Fe_2O_3 at 500°C was slightly wider than it was at 450°C, indicating that the higher calcination temperature caused the $Sm_{0.075}Fe_{0.925}$ catalyst to generate more Fe_2O_3 grain crystals. Furthermore, the interaction between samarium oxide and iron oxide was weakened, affecting the formation of iron and samarium solid solution.

3.2 Porosity and Surface Area Analysis

Table 1 shows the results of the specific surface area and pore volume of iron-based catalysts with different Sm amounts calcined at 400°C. It can be seen that the doping of Sm significantly
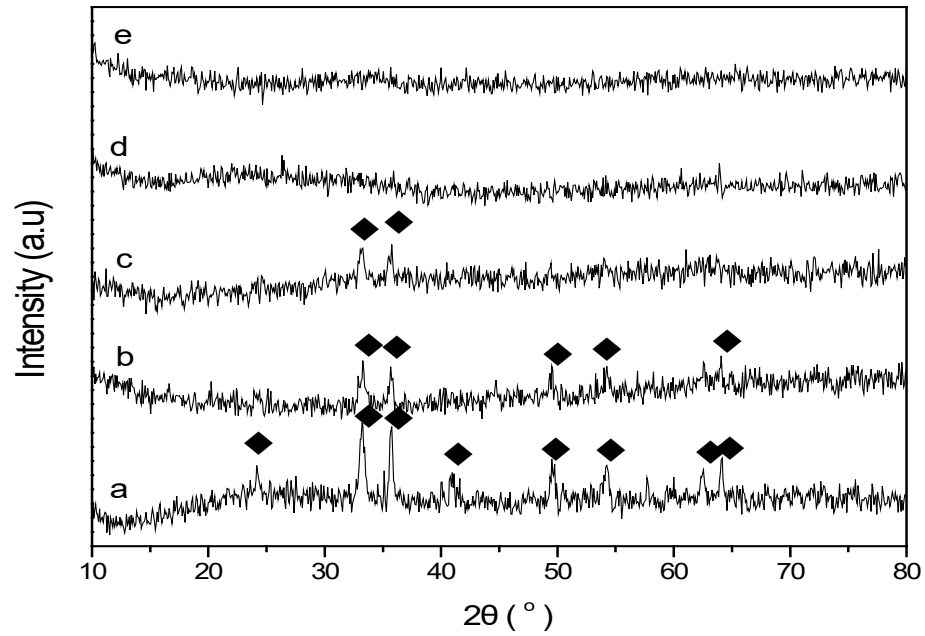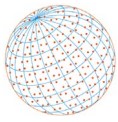
**Fig. 1.** Powder XRD patterns of SmFe mixed oxide catalysts calcined at 400°C, (a) FeO_x, (b) $Sm_{0.025}Fe_{0.975}$, (c) $Sm_{0.05}Fe_{0.95}$, (d) $Sm_{0.075}Fe_{0.925}$ and (e) $Sm_{0.1}Fe_{0.9}$.

Fig. 2. Powder XRD patterns of $Sm_{0.075}Fe_{0.925}$ catalysts calcined at different temperatures. (a) FeO_x, (b) 350°C, (c) 400°C, (d) 450°C, (e) 500°C.

Table 1. BET surface area, and pore diameter/volume of samples calcined at 400°C.

| Samples	S_{BET} ($m^2\ g^{-1}$)	Pore volume ($cm^3\ g^{-1}$)	Pore diameter (nm)
FeO_x	39	0.20	20.5
$Sm_{0.025}Fe_{0.975}$	66	0.22	13.3
$Sm_{0.05}Fe_{0.95}$	106	0.24	9.1
$Sm_{0.075}Fe_{0.925}$	124	0.25	8.0
$Sm_{0.1}Fe_{0.9}$	170	0.25	5.9
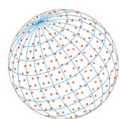
increased the specific surface area and pore volume of the iron-based catalyst. The specific surface area of pure FeO_x catalyst was only 39 m^2 g^{-1} and with the increase of doping amount, the surface area of the catalyst $Sm_{0.1}Fe_{0.9}$ increased to 170 m^2 g^{-1}. In addition, the pore volume of the catalyst gradually increased as the increases of Sm amount. Simultaneously, more mesoporous pores with smaller pore diameter generated, which could be speculated that the substitution of smaller Fe by Sm with a larger cation radius reduced the pore diameters of the catalysts. To our best knowledge, high surface area and pore volume would greatly benefit the activity of catalysts, due to offering more active sites, efficient channels for mass transport and short diffusion length of reaction gases (Zhan *et al.*, 2014a; Parlett *et al.*, 2013).

3.3 SEM

In order to investigate the effect of different precipitating agents on the morphology and particle size of the SmFe composite oxide, SEM was carried out on the $Sm_{0.075}Fe_{0.925}$ catalyst prepared with $NH_3·H_2O$ and $(NH_4)_2CO_3$ as the precipitating agent. It can be seen from the comparison of the low-magnification images in Figs. 3(A) and 3(B) that the catalyst presented large agglomeration, and the surface of the block was relatively smooth. As shown in the high-magnification images of Figs. 3(C) and 3(D) that the catalyst particles prepared with different precipitating agents were all composed of nanoparticles, and the catalyst particles prepared with $NH_3·H_2O$ were smaller. In general, the dispersion of the catalyst prepared by the two precipitating agents was not uniform, the catalyst prepared with $NH_3·H_2O$ had smaller particle size and lighter agglomeration, which may be related to the nucleation rate of the precipitate is faster compared to that prepared with $(NH_4)_2CO_3$.

3.4 XPS

Considering the influence of valence state of catalyst surface element on the deNO$_x$ activity, XPS of FeO_x and $Sm_{0.075}Fe_{0.925}$ was performed as shown in Fig. 4. Fig. 4(A) shows the Fe 2p spectra. Three prominent peaks over FeO_x catalyst were observed in the binding energy range of 705–735 eV. The peak at 709.0 eV could be attributed to the binding energy of Fe^{2+} two and the peaks at 711.6 and 724.0 eV are the binding energy of Fe^{3+} (France *et al.*, 2017; Yang *et al.*, 2011), indicating that Fe^{2+} and Fe^{3+} coexisted on the surface of FeO_x catalyst. While the less content of Fe^{2+} resulted
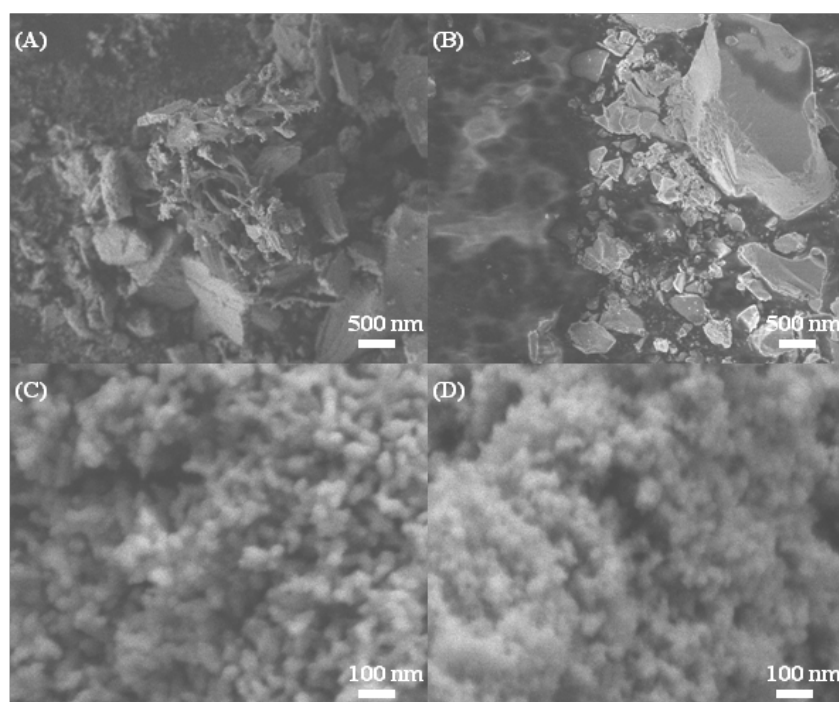

Fig. 3. SEM images of $Sm_{0.075}Fe_{0.925}$ catalyst calcined at 400°C (A) and (C) with $NH_3·H_2O$, (B) and (D) with $(NH_4)_2CO_3$.
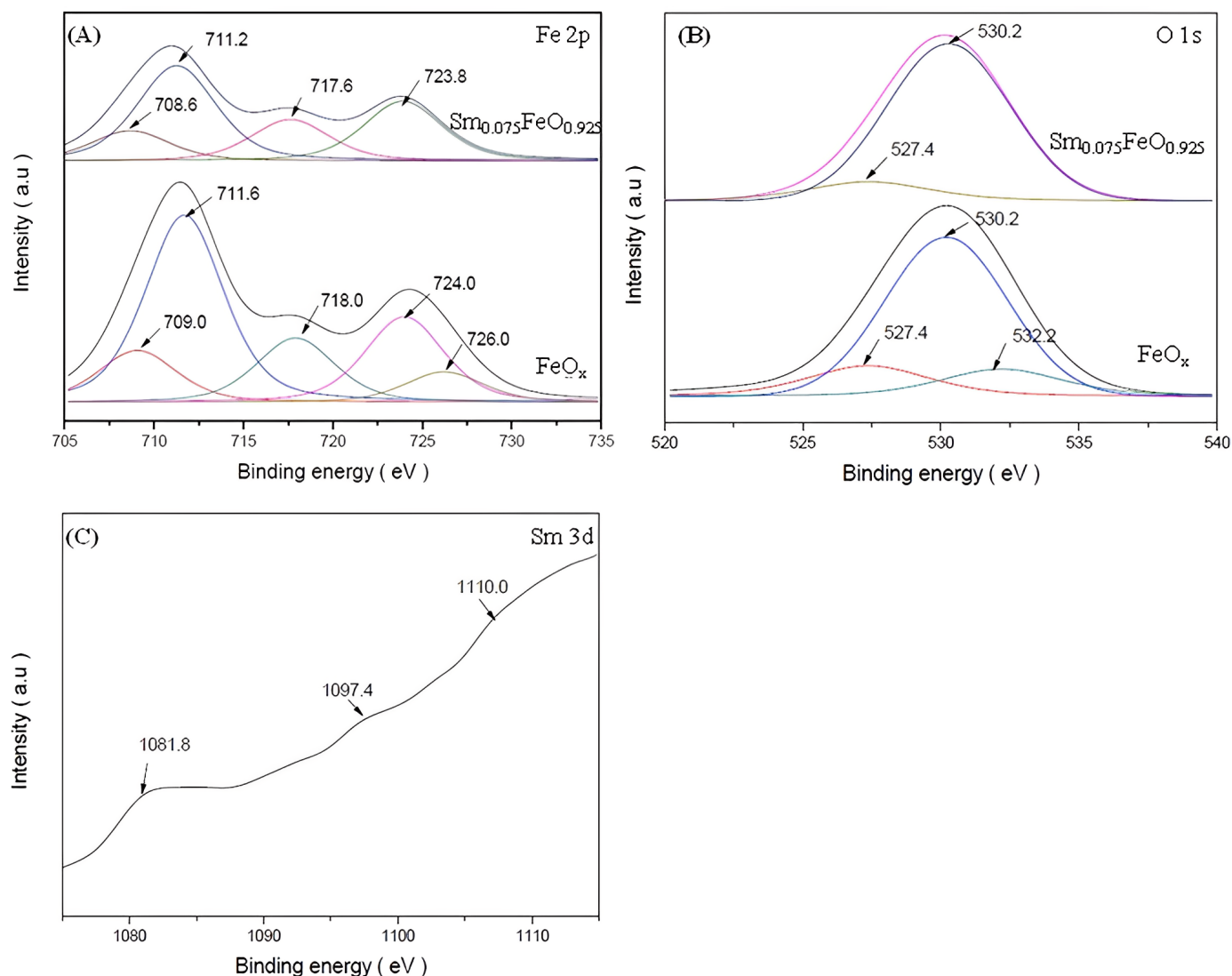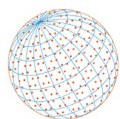
Fig. 4. XPS of (A) Fe 2p, (B) O 1s, (C) Sm 3d of FeO_x and $Sm_{0.075}Fe_{0.925}$ calcined at 400°C.

in the failure to observe divalent iron oxides in the XRD pattern (Fig. 1). After the addition of Sm, the Fe 2p XPS Gaussian fitting curve of $Sm_{0.075}Fe_{0.925}$ was similar to that of FeO_x, indicating that there were Fe^{2+} and Fe^{3+} on the surface. The binding energy for $Sm_{0.075}Fe_{0.925}$ shifted to lower values of about 0.4 eV, indicating that the addition of Sm increased the density of the electron cloud around Fe atoms, and there is a strong interaction between Sm and Fe. The O1s spectra of the catalyst are shown in Fig. 4(B). Three Gaussian simulation peaks were observed at 527.4, 530.2 and 532.2 eV on FeO_x. The peak at 527.4 and 530.2 eV were attributed to the lattice oxygen and the peak at 532.2 eV was assigned to surface adsorbed oxygen (Kang *et al.*, 2007; Parlett *et al.*, 2013). Compared with FeO_x, the chemically adsorbed oxygen at of 532.2 eV disappeared over $Sm_{0.075}Fe_{0.92}$, indicating that the addition of Sm reduced the content of chemically adsorbed oxygen on the surface. Fig. 4(C) shows the Sm3d XPS curve of $Sm_{0.075}Fe_{0.925}$. The peak at 1081.2 eV corresponds to the 3d5/2 structure of Sm^{2+}, and the peak at about 1110.0 eV is the 3d3/2 peak of Sm^{3+} (Sone *et al.*, 2015; Liu *et al.*, 2019). The weaker accompanying peak at 1097.4 eV further proved the existence of two valence states of Sm. However, the Sm^{3+} at 1084.8 eV moved about 1.6 eV to higher binding energy than the standard spectrum Sm^{3+} (1083.2 eV), indicating that the electron density around Sm atoms was decreased. This phenomenon was mutually corroborated by the increase in electron density around Fe atoms in the catalyst. This finding was related to the increase of the surrounding electron density around Fe atoms in the catalyst and further confirmed the existing strong interaction between samarium and iron.
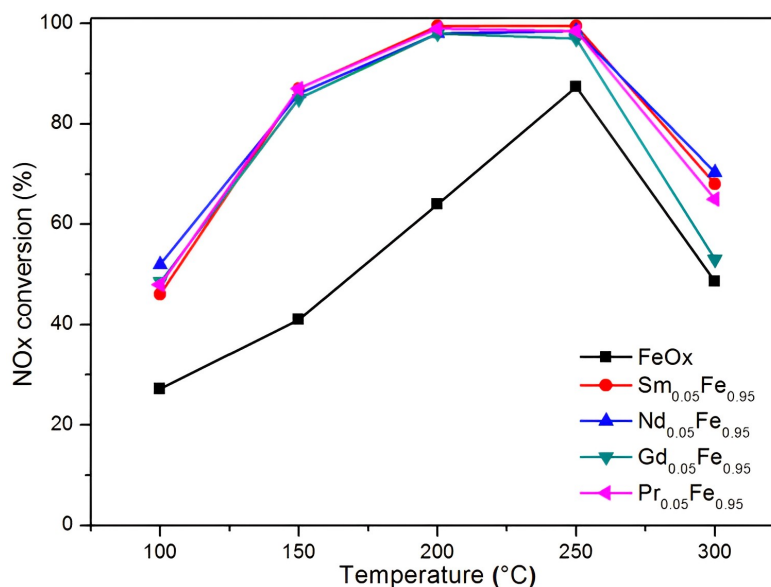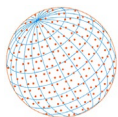
Fig. 5. Effect of different rare earth-doping (Sm, Nd, Gd and Pr) on the NH_3-SCR activity of iron oxide catalysts.

3.5 Catalytic Performance

### 3.5.1 Effect of different rare earth doping on SCR activity

Fig. 5 shows the effect of different rare earth-doped iron-based oxides on the NO_x conversion rate. As shown in Fig. 5, for pure FeO, the NO_x removal rate was only 27.2% at 100°C, reached a maximum NO_x conversion rate of 87.4% at 250°C, and then rapidly decreased. After adding four different rare earth oxides, the similar conversion curves can be seen. The NO_x conversion rate was about 50.0% at 100°C and the maximum removal rate was nearly 100% between 200–250°C. The doping of rare earth oxides significantly increased NO_x conversion rate over iron-based oxide and broadened the whole temperature window, which could be due to the existing synergistic interaction between doping and Fe species for the bi-metal oxides. In detail, the addition of rare earth oxides increased the specific surface area of the catalyst, which is conducive to the exposure of more active sites and increases the oxygen storage capacity (Qi and Yang, 2003; Tang *et al.,* 2006). Thus, more reactive gases can be quickly adsorbed on the catalyst surface and fully reacted with more active sites exposed, thereby improving the deNO$_x$ activity of the catalysts.

3.5.2 Effect of Sm amount on SCR activity

Fig. 6 shows the effect of the amount of Sm addition on the NO_x conversion rate of the iron-based catalyst. The doping in rare earth Sm oxide had a significant effect of improving the activity of the catalyst. Compare to the catalyst FeO$_x$, the NO_x conversion rate of the catalyst added a small amount of samarium oxide was significantly improved. The deNO$_x$ performance of the catalyst first increased and subsequently dropped as the ratio of doped Sm grew steadily from 0 to 0.1; the ideal doping ratio was 0.075. As the increase of Sm amount, the specific surface area and pore volume of the catalyst gradually increased (Table 1) and the optimum molar ratio of Sm doping with the best activity is 0.075. At the optimal doping rate, the deNO$_x$ rate is close to 100% between 200 and 250°C. Compared with the NO conversion (90% and 92%) of the same type of catalyst (Mn@ZIF-8 and MnO$_x$) in recent years, the conversion is higher and the reaction temperature is lower (Chen *et al.,* 2021b; Zhu *et al.,* 2021). This means structural properties are not single decisive factors affecting catalytic activity, and the composition of the catalyst would also affect the catalytic activity due to the interaction of Sm and Fe species.

3.5.3 Effect of different precipitants on SCR activity

The effect of different precipitants ($NH_3 \cdot H_2O$, $(NH_4)_2CO_3$ and NaOH) on SCR activity over $Sm_{0.075}Fe_{0.925}$ was investigated. As shown in Fig. 7, in the temperature range of 150–250°C,
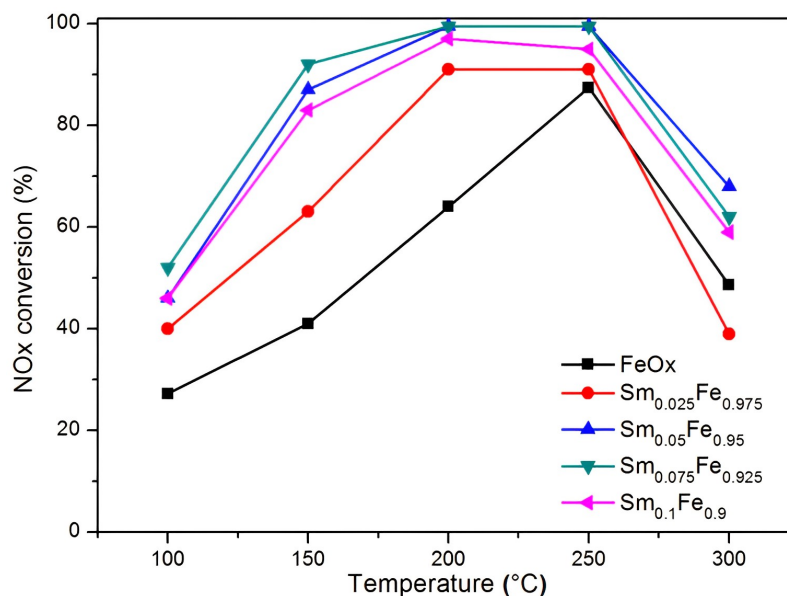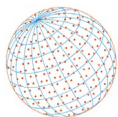
**Fig. 6.** Effect of the amount of Sm on the NH₃-SCR activity of iron oxide catalyst.
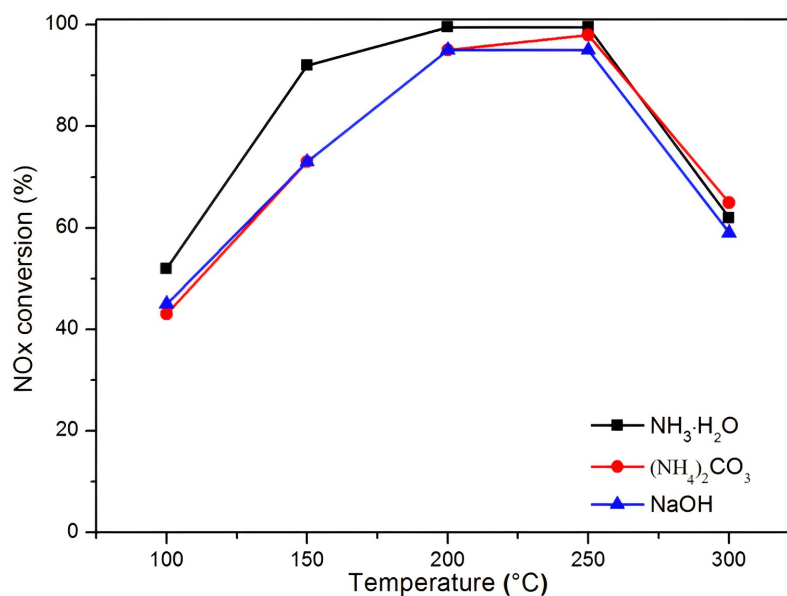
Fig. 7. Effect of precipitations on the NH₃-SCR activity of SmFe mixed oxide catalysts.

the catalyst produced with $NH_3 \cdot H_2O$ as precipitant had the highest activity with a maximum NO_x conversion exceeding 93%. There was no significant difference in the activity below 250°C for the catalyst prepared with the $(NH_4)_2CO_3$ and NaOH as the precipitating agent. In addition, at 300°C the catalyst prepared with $(NH_4)_2CO_3$ exhibited a slightly better NO_x conversion (66.7%) than the catalyst prepared with the other two precipitants, which may be due to the difference in the particle size and dispersity of catalyst. From the SEM analysis in Fig. 3, the catalyst prepared with $NH_3 \cdot H_2O$ as the precipitant had a small particle size, loose structure and good particle dispersion, meaning that particle size and dispersity could affect the SCR activity.

3.5.4 Effect of calcination temperature on SCR activity

Fig. 8 shows the effect of calcination temperature on the catalytic activity of $Sm_{0.075}Fe_{0.925}$ catalyst. The order of catalytic activity at different calcination temperatures is 350°C ≈ 400°C > 450°C > 500°C, the $Sm_{0.075}Fe_{0.925}$ achieved 100% the de-NOx efficiencies at calcination temperatures of
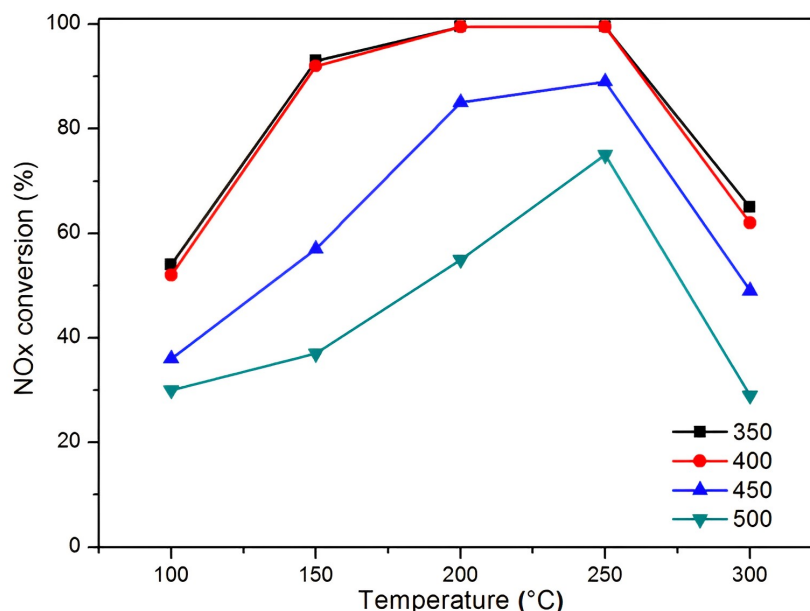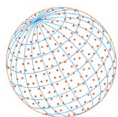
Fig. 8. Effect of calcination temperatures on NH$_3$-SCR activity of SmFe mixed oxide catalysts.
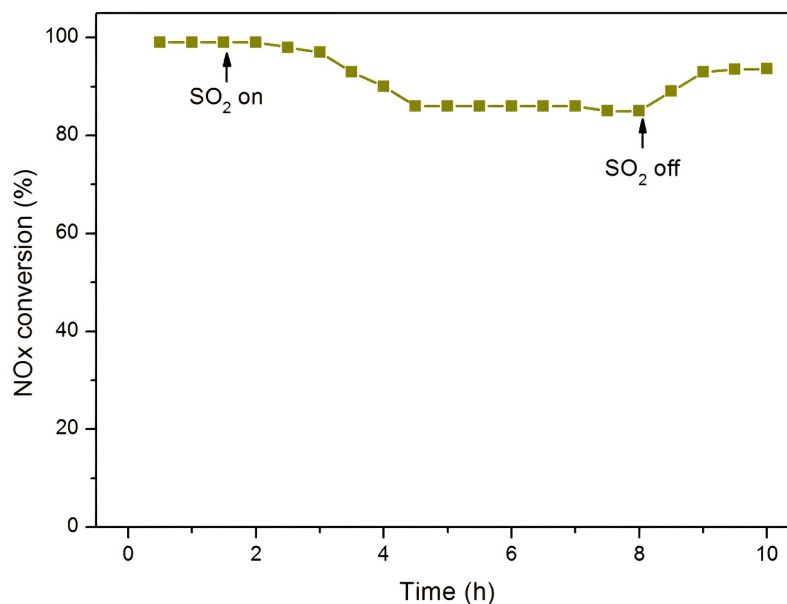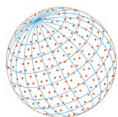
350–400°C. The catalyst's catalytic activity rapidly reduced as the calcination temperature rose. This might be because differing calcination temperatures resulted in the presence of active substances on the catalyst surface in various forms. According to the XRD pattern of the Sm$_{0.075}$Fe$_{0.925}$ catalyst that was calcined at various temperatures (Fig. 2), the diffraction peaks of Fe$_2$O$_3$ were not visible at 350°C and 400°C whereas they were present at 450°C. It should be noted when the calcination temperature raised to 500°C, the diffraction peaks of Fe$_2$O$_3$ were more obvious. A negative correlation was observed between the crystalline phase strength of Fe$_2$O$_3$ on the surface of the catalysts and their catalytic activity. Based on the previous reports, the low crystallization or amorphous phase for composite oxides catalysts is responsible for SCR activity due to short-range ordered structure in the location of active sites (Li *et al.*, 2012; Xin *et al.*, 2018). Thus, a reasonable explanation can be drawn that as the calcination temperature increased, finer Fe$_2$O$_3$ phases were precipitated on the catalysts, which decreased the amount of solid solution formed by Fe and Sm components and weakened the interaction between samarium oxide and iron oxide, reducing the activity of the catalysts.

3.5.5 Effect of SO$_2$ on SCR activity

A tiny quantity of SO$_2$ is typically present in the flue gas during industrial application, which causes the catalyst to become inactive. So, at 200°C, the impact of SO$_2$ on the SCR activity of Sm$_{0.025}$Fe$_{0.975}$ was examined. As shown in Fig. 9, when 0.05% SO$_2$ was added to the reaction gases, the NO$_x$ conversion slowly decreased and then stabilized. The NO$_x$ conversion decreased from 99% of the initial value to about 86% then recovered to about 94% after SO$_2$ was removed about 1 h, which was slightly lower than the initial value, indicating that the catalyst was partially deactivated. According to the literature (Wang *et al.*, 2020b), this might be a result of the catalyst developing ammonium sulfate or ammonium bisulfate on its surface, which clogged the pores and took up the catalyst's active sites, decreasing its activity.

4 CONCLUSIONS

(1) The doping of rare earth oxides significantly improved the iron-based oxides with similar NO$_x$ removal efficiency.
(2) With the increase of rare earth Sm, the deNO$_x$ efficiency of the catalyst first increased and then decreased. Sm$_{0.075}$Fe$_{0.925}$O$_x$ catalyst exhibited the highest activity, resulting from the improved structural properties and component interaction.

Fig. 9. Effect of SO_2 on the SCR activity of $Sm_{0.025}Fe_{0.975}$ catalyst.

(3) The catalyst activity was significantly impacted by the calcination temperature. The order of catalytic activity is $350°C \approx 400°C > 450°C > 500°C$. This is due to the decreased solid solution formed by Fe and Sm components and weakened interaction between samarium oxide and iron oxide, reducing the activity of the catalysts.

(4) The catalyst prepared by using $NH_3 \cdot H_2O$ as the precipitating agent exhibited better activity than that of the catalyst prepared by $(NH_4)_2CO_3$ and NaOH.

(5) When adding 0.05% SO_2, the $deNO_x$ efficiency was decreased to 86% from 98% and recovered to 93% after SO_2 was removed, indicating the $Sm_{0.075}Fe_{0.925}$ catalyst can be basically regenerated.

CONFLICTS OF INTEREST

The authors declare the following competing financial interest(s): Rui Wang and Ying Wei declare a financial interest. A Chinese patent related to this research has been authorized (ZL201410195455.3).

ACKNOWLEDGEMENTS

REFERENCES

Brandenberger, S., Kroecher, O., Casapu, M., Tissler, A., Althoff, R. (2011). Hydrothermal deactivation of Fe-ZSM-5 catalysts for the selective catalytic reduction of NO with NH_3. Appl. Catal., B 101, 649–659. https://doi.org/10.1016/j.apcatb.2010.11.006

Chen, J., Qu, W., Chen, Y., Liu, X., Jiang, X., Wang, H., Zong, Y., Ma, Z., Tang, X. (2018). Simultaneously enhancing stability and activity of maghemite via site-specific Ti(IV) doping for NO emission control. ChemCatChem 10, 4683–4688. https://doi.org/10.1002/cctc.201801169

Chen, J., Fu, P., Lv, D., Chen, Y., Fan, M., Wu, J., Meshram, A., Mu, B., Li, X., Xia, Q. (2021a). Unusual positive effect of SO_2 on Mn-Ce mixed-oxide catalyst for the SCR reaction of NO_x with NH_3. Chem. Eng. J. 407, 127071. https://doi.org/10.1016/j.cej.2020.127071

Chen, Y., Yu, M., Wang, R. (2021b). Porous zeolitic imidazolate framework loaded Mn as an
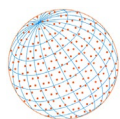
efficient catalyst for the selective catalytic reduction of NO$_x$ with NH$_3$. Aerosol Air Qual. Res. 21, 210201. https://doi.org/10.4209/aaqr.210201

Da Silva, E.L., Marinopoulos, A.G., Vieira, R.B.L., Vilão, R.C., Alberto, H.V., Gil, J.M., Lichti, R.L., Mengyan, P.W., Baker, B.B. (2016). Electronic structure of interstitial hydrogen in lutetium oxide from DFT+U calculations and comparison study with μSR spectroscopy. Phys. Rev. B 94, 014104. https://doi.org/10.1103/PhysRevB.94.014104

Eigenmann, F., Maciejewski, M., Baiker, A. (2006). Selective reduction of NO by NH$_3$ over manganese-cerium mixed oxides: Relation between adsorption, redox and catalytic behavior. Appl. Catal., B 62, 311–318. https://doi.org/10.1016/j.apcatb.2005.08.005

Fan, Z., Shi, J.W., Gao, C., Gao, G., Wang, B., Niu, C. (2017). Rationally designed porous MnO$_x$-FeO$_x$ Nanoneedles for low-temperature selective catalytic reduction of NO$_x$ by NH$_3$. ACS Appl. Mater. Interfaces 9, 16117–16127. https://doi.org/10.1021/acsami.7b00739

France, L.J., Yang, Q., Li, W., Chen, Z., Guang, J., Guo, D., Wang, L., Li, X. (2017). Ceria modified FeMnO$_x$–Enhanced performance and sulphur resistance for low-temperature SCR of NO$_x$. Appl. Catal., B 206, 203–215. https://doi.org/10.1016/j.apcatb.2017.01.019

Guo, Y., Lu, G. (2007). Current status and some perspectives of rare earth catalytic materials. J. Chin. Rare Earth Soc. 25, 1–15.

Han, L., Cai, S., Gao, M., Hasegawa, J., Wang, P., Zhang, J., Shi, L., Zhang, D. (2019). Selective catalytic reduction of NO$_x$ with NH$_3$ by using novel catalysts: State of the art and future prospects. Chem. Rev. 119, 10916–10976. https://doi.org/10.1021/acs.chemrev.9b00202

Jayashree, M., Parthibavarman, M., Prabhakaran, S. (2019). Hydrothermal-induced alpha-Fe$_2$O$_3$/graphene nanocomposite with ultrahigh capacitance for stabilized and enhanced supercapacitor electrodes. Ionics 25, 3309–3319. https://doi.org/10.1007/s11581-019-02859-z

Kang, M., Park, E.D., Kim, J.M., Yie, J.E. (2007). Manganese oxide catalysts for NO$_x$ reduction with NH$_3$ at low temperatures. Appl. Catal., A 327, 261–269. https://doi.org/10.1016/j.apcata.2007.05.024

Kobayashi, M., Miyoshi, K. (2007). WO$_3$-TiO$_2$ monolithic catalysts for high temperature SCR of NO by NH$_3$: Influence of preparation method on structural and physico-chemical properties, activity and durability. Appl. Catal., B 72, 253–261. https://doi.org/10.1016/j.apcatb.2006.11.007

Kompio, P.G.W.A., Brueckner, A., Hipler, F., Auer, G., Loeffler, E., Gruenert, W. (2012). A new view on the relations between tungsten and vanadium in V$_2$O$_5$-WO$_3$/TiO$_2$ catalysts for the selective reduction of NO with NH$_3$. J. Catal. 286, 237–247. https://doi.org/10.1016/j.jcat.2011.11.008

Kroecher, O., Elsener, M. (2008). Chemical deactivation of V$_2$O$_5$/WO$_3$-TiO$_2$ SCR catalysts by additives and impurities from fuels, lubrication oils, and urea solution: I. Catalytic studies. Appl. Catal., B 77, 215–227. https://doi.org/10.1016/j.apcatb.2007.04.021

Li, G., Wang, B., Wang, H., Ma, J., Xu, W.Q., Li, Y., Han, Y., Sun, Q. (2018). Fe and/or Mn oxides supported on fly ash-derived SBA-15 for low-temperature NH$_3$-SCR. Catal. Commun. 108, 82–87. https://doi.org/10.1016/j.catcom.2018.01.035

Li, P., Xin, Y., Li, Q., Wang, Z., Zhang, Z., Zheng, L. (2012). Ce-Ti amorphous oxides for selective catalytic reduction of NO with NH$_3$: Confirmation of Ce-O-Ti active sites. Environ. Sci. Technol. 46, 9600–9605. https://doi.org/10.1021/es301661r

Liu, F., He, H., Zhang, C. (2008). Novel iron titanate catalyst for the selective catalytic reduction of NO with NH$_3$ in the medium temperature range. Chem. Commun. 2043–2045. https://doi.org/10.1039/B800143J

Liu, F., He, H., Ding, Y., Zhang, C. (2009). Effect of manganese substitution on the structure and activity of iron titanate catalyst for the selective catalytic reduction of NO with NH$_3$. Appl. Catal., B 93, 194–204. https://doi.org/10.1016/j.apcatb.2009.09.029

Liu, H., Fan, Z., Sun, C., Yu, S., Feng, S., Chen, W., Chen, D., Tang, C., Gao, F., Dong, L. (2019). Improved activity and significant SO$_2$ tolerance of samarium modified CeO$_2$-TiO$_2$ catalyst for NO selective catalytic reduction with NH$_3$. Appl. Catal., B 244, 671–683. https://doi.org/10.1016/j.apcatb.2018.12.001

Meng, D., Zhan, W., Guo, Y., Guo, Y., Wang, L., Lu, G. (2015). A highly effective catalyst of Sm-MnO$_x$ for the NH$_3$-SCR of NO$_x$ at low temperature: Promotional role of Sm and its catalytic performance. ACS Catal. 5, 5973–5983. https://doi.org/10.1021/acscatal.5b00747

Meng, D., Zhan, W., Guo, Y., Guo, Y., Wang, Y., Wang, L., Lu, G. (2016). A highly effective catalyst of Sm-Mn mixed oxide for the selective catalytic reduction of NO$_x$ with ammonia: Effect of the
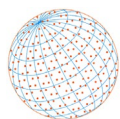
calcination temperature. J. Mol. Catal. A: Chem. 420, 272–281. https://doi.org/10.1016/j.molcata.2016.04.028

Parlett, C.M.A., Wilson, K., Lee, A.F. (2013). Hierarchical porous materials: Catalytic applications. Chem. Soc. Rev. 42, 3876–3893. https://doi.org/10.1039/c2cs35378d

Qi, G., Yang, R.T. (2003). A superior catalyst for low-temperature NO reduction with NH_3. Chem. Commun. 848–849. https://doi.org/10.1039/B212725C

Ruggeri, M.P., Selleri, T., Colombo, M., Nova, I., Tronconi, E. (2015). Investigation of NO_2 and NO interaction with an Fe-ZSM-5 catalyst by transient response methods and chemical trapping techniques. J. Catal. 328, 258–269. https://doi.org/10.1016/j.jcat.2015.02.003

Shan, W., Liu, F., He, H., Shi, X., Zhang, C. (2012). A superior Ce-W-Ti mixed oxide catalyst for the selective catalytic reduction of NO_x with NH_3. Appl. Catal., B 115, 100–106. https://doi.org/10.1016/j.apcatb.2011.12.019

Shwan, S., Jansson, J., Korsgren, J., Olsson, L., Skoglundh, M. (2012). Kinetic modeling of H-BEA and Fe-BEA as NH_3-SCR catalysts-effect of hydrothermal treatment. Catal. Today 197, 24–37. https://doi.org/10.1016/j.cattod.2012.06.014

Shwan, S., Jansson, J., Olsson, L., Skoglundh, M. (2015). Deactivation mechanisms of iron-exchanged zeolites for NH_3-SCR applications. Catal. Today 258, 432–440. https://doi.org/10.1016/j.cattod.2015.01.003

Sone, B.T., Manikandan, E., Gurib-Fakim, A., Maaza, M. (2015). Sm_2O_3 nanoparticles green synthesis via Callistemon viminalis' extract. J. Alloys Compd. 650, 357–362. https://doi.org/10.1016/j.jallcom.2015.07.272

Sun, C., Chen, W., Jia, X., Liu, A., Gao, F., Feng, S., Dong, L. (2021). Comprehensive understanding of the superior performance of Sm-modified Fe_2O_3 catalysts with regard to NO conversion and H_2O/SO_2 resistance in the NH_3-SCR reaction. Chin. J. Catal. 42, 417–430. https://doi.org/10.1016/s1872-2067(20)63666-x

Tan, W., Liu, A., Xie, S., Yan, Y., Shaw, T.E., Pu, Y., Guo, K., Li, L., Yu, S., Gao, F., Liu, F., Dong, L. (2021). Ce-Si mixed oxide: A high sulfur resistant catalyst in the NH_3-SCR reaction through the mechanism-enhanced process. Environ. Sci. Technol. 55, 4017–4026. https://doi.org/10.1021/acs.est.0c08410

Tang, X., Hao, J., Xu, W., Li, J. (2006). Novel MnO_x catalyst for low-temperature selective catalytic reduction of NO_x with NH_3. Chin. J. Catal. 27, 843–848.

Wang, H., Ning, P., Zhang, Y., Ma, Y., Wang, J., Wang, L., Zhang, Q. (2020a). Highly efficient WO_3-FeO_x catalysts synthesized using a novel solvent-free method for NH_3-SCR. J. Hazard. Mater. 388. https://doi.org/10.1016/j.jhazmat.2019.121812

Wang, Q., Zhou, J., Zhang, J., Zhu, H., Feng, Y., Jin, J. (2020b). Effect of ceria doping on catalytic activity and SO_2 resistance of MnO_x/TiO_2 catalysts for selective catalytic reduction of NO with NH_3 at low temperature. Aerosol Air Qual. Res. 20, 477–488. https://doi.org/10.4209/aaqr.2019.10.0546

Wei, Y. (2014). Study on Iron Oxide Catalysts Modified by Rare Earth for NH_3-SCR of NO_x. Shandong University. https://kns.cnki.net/KCMS/detail/detail.aspx?dbname=CMFD201402&filename=1014313670.nh (in Chinese)

Xin, Y., Zhang, N., Li, Q., Zhang, Z., Cao, X., Zheng, L., Zeng, Y., Anderson, J.A. (2018). Selective catalytic reduction of NO_x with NH_3 over short-range ordered W-O-Fe structures with high thermal stability. Appl. Catal., B 229, 81–87. https://doi.org/10.1016/j.apcatb.2018.02.012

Xiong, Z., Lu, C., Guo, D., Zhang, X., Han, K. (2013). Selective catalytic reduction of NO_x with NH_3 over iron-cerium mixed oxide catalyst: Catalytic performance and characterization. J. Chem. Technol. Biotechnol. 88, 1258–1265. Https://Doi.Org/10.1002/Jctb.3966

Xue, D., Sun, C., Chen, X. (2017). Hybridized valence electrons of $4f^{0-14}5d^{0-1}6s^2$: The chemical bonding nature of rare earth elements. J. Rare Earths 35, 837–843. https://doi.org/10.1016/s1002-0721(17)60984-0

Yang, S., Wang, C., Li, J., Yan, N., Ma, L., Chang, H. (2011). Low temperature selective catalytic reduction of NO with NH_3 over Mn-Fe spinel: Performance, mechanism and kinetic study. Appl. Catal., B 110, 71–80. https://doi.org/10.1016/j.apcatb.2011.08.027

Yang, S., Liu, C., Chang, H., Ma, L., Qu, Z., Yan, N., Wang, C., Li, J. (2013). Improvement of the activity of γ-Fe_2O_3 for the selective catalytic reduction of NO with NH_3 at high temperatures: NO reduction versus NH_3 oxidization. Ind. Eng. Chem. Res. 52, 5601–5610. https://doi.org/10.1021/ie303272u
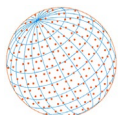
Zhan, S., Qiu, M., Yang, S., Zhu, D., Yu, H., Li, Y. (2014a). Facile preparation of MnO_2 doped Fe_2O_3 hollow nanofibers for low temperature SCR of NO with NH_3. J. Mater. Chem. A 2, 20486–20493. https://doi.org/10.1039/c4ta04807e

Zhan, W., Guo, Y., Gong, X., Guo, Y., Wang, Y., Lu, G. (2014b). Current status and perspectives of rare earth catalytic materials and catalysis. Chinese J. Catal. 35, 1238–1250. https://doi.org/10.1016/s1872-2067(14)60189-3

Zhang, J., Huang, Z., Du, Y., Wu, X., Shen, H., Jing, G. (2020). Atomic-scale insights into the nature of active sites in Fe_2O_3-supported submonolayer WO_3 catalysts for selective catalytic reduction of NO with NH_3. Chem. Eng. J. 381. https://doi.org/10.1016/j.cej.2019.122668

Zhu, H., Qiu, L., Wang, R. (2021). Insights into reaction conditions for selective catalytic reduction of NO_x with a MnAl oxide catalyst at low temperatures. Aerosol Air Qual. Res. 21, 210066. https://doi.org/10.4209/aaqr.210066